Letters

ESR Modeling of Class II MLCC Large-Signal-Excitation Losses

David Menzi, *Member, IEEE*, Shmuel Ben-Yaakov, *Fellow, IEEE*, Grayson Zulauf, *Member, IEEE*, and Johann W. Kolar, *Fellow, IEEE*

***Abstract*—Multilayer ceramic capacitors (MLCCs) with ferroelectric Class II dielectrics enable extremely high volumetric capacitance density, and are therefore preferred in high-power-density power conversion. These MLCCs, though, suffer from a nonlinear dielectric constant and substantial low-frequency, large-signal excitation losses. Previously, a Steinmetz-parameter-based loss model accurately described these large-signal losses in MLCCs, but a difficult peak-charge measurement was required. For magnetic materials, a Steinmetz-based model is translated to an operating-point-specific effective series resistance (ESR) model, which then allows for a low-complexity loss calculation. In this letter, we introduce and verify an ESR-based loss model for MLCCs, with the ESR derived from the MLCC Steinmetz parameters. Our modeling error is below 25% across all evaluated operating points, a major improvement over modeling with the small-signal ESR provided in the MLCC datasheet, which may result in a loss approximation error of up to 10×.**

***Index Terms*—AC-DC power converters, DC–AC power converters, effective series resistance (ESR), IGSE, IGSE-C, inverters, loss modeling, multilayer ceramic capacitors (MLCCs) , power capacitors, rectifiers, Steinmetz equation.**

I. Introduction

CLASS II ferroelectric multilayer ceramic capacitors (MLCCs) feature a high (relative) dielectric constant, enabling extremely high volumetric capacitance density [1], [2], [3] and making them the preferred capacitor technology for ultra-compact power converter systems [4], [5]. These Class II MLCCs, though, exhibit nonlinear dielectric constants (as shown in Fig. 1) and suffer from losses from low-frequency, large-signal excitations [6], [7], [8] that result in lower converter efficiency and may cause fatal MLCC overheating. Accurately modeling these losses, therefore, is critically important for both optimization and reliability in power converter design.

Manuscript received 15 December 2022; revised 18 January 2023; accepted 11 February 2023. Date of publication 17 February 2023; date of current version 10 March 2023. *(Corresponding author: David Menzi.)*

David Menzi is with the Power Electronic Systems Laboratory (PES), ETH Zurich, 8092 Zurich, Switzerland (e-mail: menzi@lem.ee.ethz.ch).

Shmuel Ben-Yaakov is with the Ben-Gurion University of the Negev, Beer-Sheva 84105, Israel (e-mail: sam.benyaakov@gmail.com).

Grayson Zulauf is with the Resonant Link Inc., Palo Alto, CA 94301 USA (e-mail: grayson.d.zulauf@gmail.com).

Johann W. Kolar is with the Power Electronic Systems Laboratory (PES), ETH Zurich, 8044 Zurich, Switzerland (e-mail: kolar@lem.ee.ethz.ch).

Color versions of one or more figures in this article are available at https://doi.org/10.1109/TPEL.2023.3246095.

Digital Object Identifier 10.1109/TPEL.2023.3246095

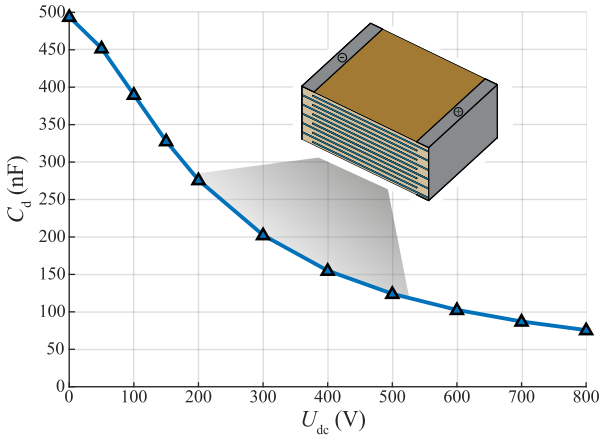

Fig. 1. Small-signal / differential capacitance C_d over dc-bias voltage U_{dc} of a 1 kV/470 nF MLCC (2220Y1K00474KETWS2).

Existing loss models for Class II MLCCs under large-signal excitations suffer from the shortcomings traditional with loss modeling for nonlinear passive components, including lack of extensibility, the need for difficult and time-consuming measurements, and lack of accuracy. More specifically, existing loss models can be categorized as as follows.

1) *Lookup Tables* [7], [8] that provide measured losses for a set of operating points (e.g., for different dc-bias and ac voltage amplitude values). These lookup tables support interpolation to predict expected MLCC losses but cannot be applied across different voltage waveforms.
2) *Equivalent Series Resistance (ESR)- or Loss-Tangent-Based Models* [6] are widely used in the industry since they allow a straightforward loss calculation based on the excitation rms current and/or voltage that can be easily measured. The equivalent series resistance (ESR) data typically available in the MLCC datasheet, though, does not accurately describe the loss behavior of Class II MLCCs under large-signal excitation [9], [10], [11], and a large set of measurement-based ESR values is required (similar to a loss-map-based approach) for an accurate loss calculation.
3) *Steinmetz-Based Models* [12], [13] based on the power-law relationship between MLCC losses and peak charge excitation allow an accurate loss calculation for various

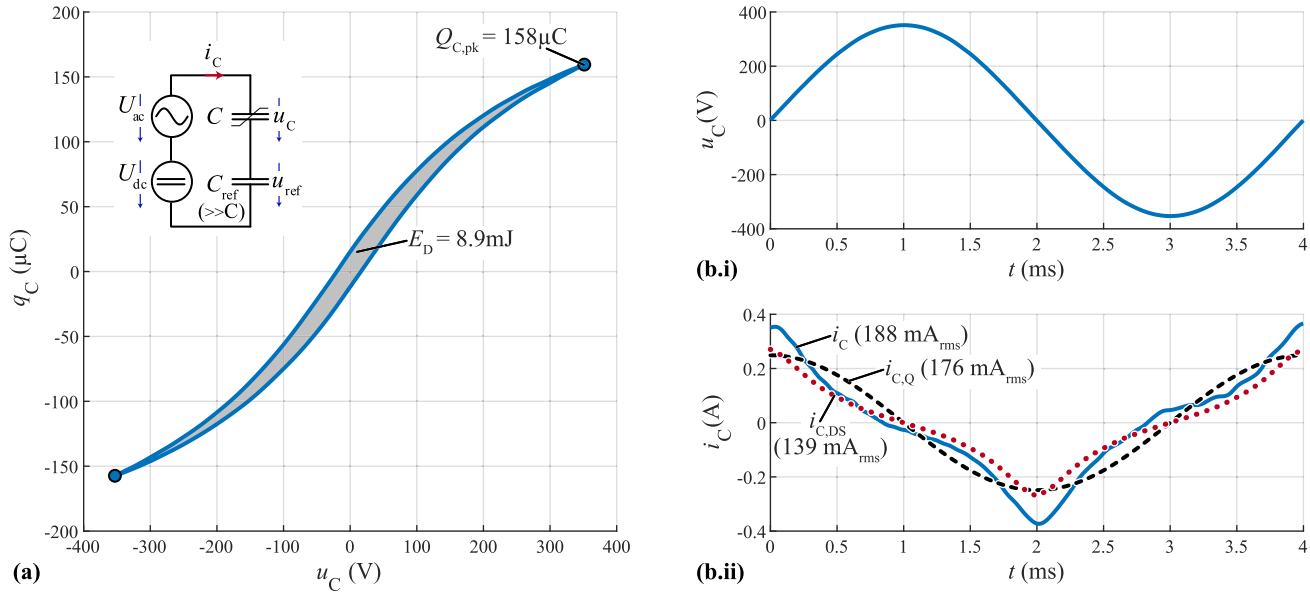

Fig. 2. (a) Measured voltage-charge ($U_C - Q_C$) hysteresis (and employed Sawyer–Tower measurement setup [12]) and (b) corresponding time-domain waveforms of voltage u_C (b.i) and current i_C (b.ii) of a 1 kV / 470 nF MLCC (2220Y1K00474KETWS2) excited with $U_{ac} = 270$ V$_{rms}$ at f =250 Hz. The hysteresis area in (a) represents the dissipated energy E_D within an ac cycle and corresponds to an average power loss of 2.2 W. For comparison, (b.ii) also shows the peak-charge equivalent sinusoidal current $i_{C,Q}$ ($I_{C,Q} = 176$ mA$_{rms}$), the measured, nonsinusoidal MLCC current i_C ($I_C = 188$ mA$_{rms}$), and the current $i_{C,DS}$ ($I_{C,DS} = 139$ mA$_{rms}$) calculated from the small-signal differential capacitance of Fig. 1.

voltage and current waveforms but are not straightforward to apply in practice as the (nonlinear) MLCC charge is not trivial to assess.

For ferromagnetic transformer core materials, Steinmetz-based loss models [14] are widely used. Therefore, aiming at a straightforward loss calculation, operating-point-specific ESR values are derived from the Steinmetz parameters [15], [16]. Considering that the ESR model is probably the most desirable modeling approach, research is needed to explore the ferroelectric Class II MLCC losses in terms of operating-point-specific ESR values, preferably by linking the ESR values to an already proven loss model.

In this letter, we transform the Steinmetz-based loss models [12], [13] to an operating-point-specific ESR model for MLCCs, building on the proposal for this method in [17]: we show that for typical large-signal excitation voltage waveforms, the rms value of the measured (nonsinusoidal) MLCC current and the rms value of a sinusoidal peak-charge-equivalent current are sufficiently close such that operating-point-specific MLCC ESR values can be derived based upon the MLCC Steinmetz parameters available in literature [12], [13]. Thereby, the advantages of an ESR model (i.e., a straight forward loss calculation based on the measured rms current) and of a peak-charge-based Steinmetz model (i.e., an accurate loss calculation) are combined, accordingly simplifying the accurate MLCC loss calculation substantially.

The rest of this letter is structured as follows: In Section II, we derive the Steinmetz-based ESR model for MLCCs, and validate the model with experimental measurements in Section III. Section IV utilizes the proposed model for the design example of a 3-kW motor drive inverter. Finally, Section V concludes this article.

II. Steinmetz-Based ESR Derivation

The losses in a Class II ferroelectric MLCC can be depicted with the voltage-charge ($U_C - Q_C$) hysteresis loop, which is shown in Fig. 2(a) for the capacitor C under test, (Knowles Syfer 2220Y1K00474KETWS2 with 1 kV / 470 nF).

The energy dissipated during one charge–discharge cycle E_D is defined by the area enclosed by the ($U_C - Q_C$) hysteresis loop. These MLCC large-signal excitation losses P were shown in [12] and [13] to fit a power law with the peak-charge excitation $Q_{C,pk}$ as

$$P = k \cdot f^{\alpha} \cdot Q_{C,pk}^{\beta} \tag{1}$$

with frequency f and the Steinmetz parameters from [12] with $k = 1.06 \cdot 10^6$, $\alpha = 1.0$, and $\beta = 2.12$ (for this capacitor).

While accurate, this Steinmetz model suffers from the disadvantage that the MLCC charge $Q_{C,pk}$ is not easy to measure, as the capacitance may depend on the large-signal excitation and operating point. As we discussed in Section I, an ESR-based model would be preferred since the MLCC rms current I_C is straightforward to measure. A single ESR value, though, cannot capture the nonlinear loss behavior of a ferroelectric Class II MLCC [10], [11], and the model must be extended.

As used in magnetic material loss modeling [16], the ESR can be derived from the Steinmetz parameters for a given operating point. The derivation of this operating-point-specific ESR value is based on an approximation of the nonlinear and nonsinusoidal MLCC current i_C by means of a sinusoidal-peak-charge-equivalent current $i_{C,Q}$ (peak charge is denoted as $Q_{C,pk}$) with an rms value

$$I_{C,Q} = \sqrt{2} \cdot \pi \cdot f \cdot Q_{C,pk} \cdot \approx I_C. \tag{2}$$

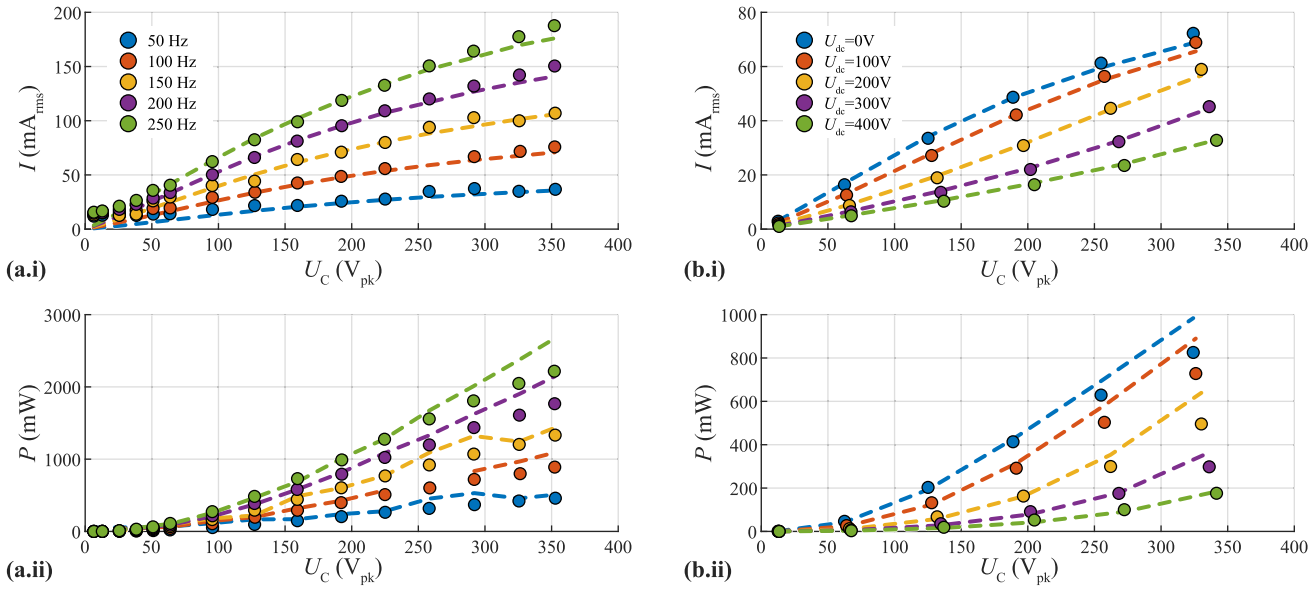

Fig. 3. Experimental data for a 1 kV/470 nF MLCC (2220Y1K00474KETWS2) to investigate the impact of (a) excitation voltage amplitude $\hat{U}_C$ and frequency f (dc bias is kept constant at $U_{dc} = 0$ V), and (b) voltage amplitude $\hat{U}_C$ and dc bias voltage U_{dc} (for a fixed frequency $f = 100$ Hz) on (a.i) and (b.i) the MLCC rms current stresses I_C and (a.ii) and (b.ii) the power MLCC losses P. In (a.i) and (b.i), the scatter points represent the measured rms current I_C and the dashed lines represent the calculated MLCC current $I_{C,Q}$ based on the measured peak charge $Q_{C,pk}$ and (2). In (a.ii) and (b.ii), the scatter points represent the measured losses and the dashed lines represent the calculated losses based on the measured rms current I_C and the operating-point-specific ESR value according to (5) with the Steinmetz parameters $k = 1.06 \cdot 10^6$, $\alpha = 1.0$, and $\beta = 2.12$.

This rms current corresponds to capacitor losses P based on ESR as

$$P = \mathrm{ESR} \cdot I_C^2 \approx \mathrm{ESR} \cdot I_{C,Q}^2. \tag{3}$$

Alternatively, the losses P obtained from the peak-charge-based Steinmetz model (1) can be translated with (2) into

$$P = k_Q \cdot f^{\alpha-\beta} \cdot \frac{I_{C,Q}^{\beta}}{\left(\sqrt{2}\pi\right)^{\beta}} \approx k_Q \cdot f^{\alpha-\beta} \cdot \frac{I_C^{\beta}}{\left(\sqrt{2}\pi\right)^{\beta}}. \tag{4}$$

And, therefore, the operating-point-dependent ESR value can be calculated from the Steinmetz parameters and the measured rms MLCC current I_C with (3) and (4) as

$$\mathrm{ESR} = k_Q \cdot f^{\alpha-\beta} \cdot \frac{I_C^{\beta-2}}{\left(\sqrt{2}\pi\right)^{\beta}}. \tag{5}$$

This equation relies on the sinusoidal current assumption, as mentioned, and the assumption that the linear MLCC peak charge $Q_{C,pk}$ to rms current I_C ratio (2) holds, which is investigated in the next section.

III. Experimental Verification

The proposed model depends upon the time-domain voltage and current measurements of the MLCC, which are shown in Fig. 2(b). The employed Sawyer–Tower [18], [19] test setup to measure the MLCC voltage u_C and charge q_C is shown in Fig. 2(a) and the MLCC current i_C is measured with a current clamp. Note that the reference capacitor C_{ref} is linear such that the charge of the device under test C is defined by $q_C = q_{ref} = u_{ref} \cdot C_{ref}$. Here, C_{ref} acts as a capacitive shunt and it is hence important to select a low-loss (e.g., with a C0G dielectric) capacitor for the realization of C_{ref} (more details on the setup are provided in [12]).

The time-domain waveforms of Fig. 2(b) correspond to the $U_C - Q_C$ hysteresis loop in Fig. 2(a). There, $i_{C,Q}(t)$ represents the peak-charge-equivalent sinusoidal current [according to (2)], and the estimated rms value $I_{C,Q}$ deviates by less than 10% from the measured current I_C.

For completeness, the MLCC current waveform $i_{C,DS}(t)$ expected from the small-signal differential capacitance C_d of Fig. 1 is

$$i_{C,DS}(t) = C_d(u_C)\frac{u_C(t)}{\mathrm{d}t}. \tag{6}$$

This small-signal-predicted current is shown in Fig. 2(b). The rms current predicted from this value, $I_{C,DS}$, differs by almost 30% from the measured value I_C, as the large-signal capacitance behavior differs substantially from the small-signal behavior under dc bias. We see, then, that the MLCC rms current I_C must be measured and cannot be calculated from datasheet information.

We next present measured data to validate the approximation (2) across excitation amplitude $\hat{U}_C$, frequency f, and dc bias voltage U_{dc}. Fig. 3(a.i) shows the measured rms current I_C (scatter points) and the estimated rms current $I_{C,Q}$ (dashed lines) across MLCC voltage $U_{C,pk}$ for excitation frequencies up to $f = 250$ Hz. The deviation remains below 10% for the full excitation voltage range across frequency. Because this deviation is minimal, the measured power losses P [Fig. 3(a.ii), scatter points] closely match the calculated losses according to (3)

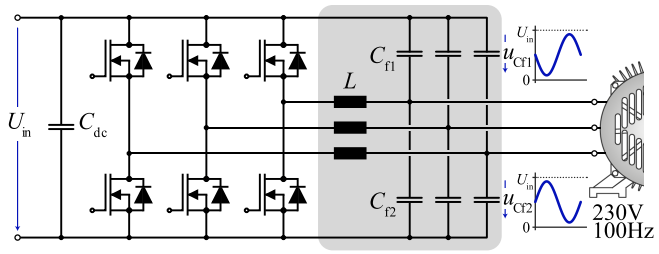

Fig. 4. Design example: inverter sinewave output filter to reduces the high-frequency stresses of a 230 V_{rms}/100 Hz three-phase machine, with positive C_{f1} and negative C_{f2} dc-link-referenced filter capacitors [20], [21].

and (4) (dashed lines), with a deviation below 25% for every operating point.

It should be noted that at high excitation voltage and frequency values (i.e., higher current) there is an increase in the deviation between the measured rms current I_C and the estimated rms current $I_{C,Q}$ in Fig. 3(a.i), as well as between the measured losses and the ESR-model calculated losses in Fig. 3(a.ii). Furthermore, the errors in the two cases are in the opposite direction. This can be explained by the fact that the employed ESR value (5) bases on $Q_{C,pk}$ and the charge-equivalent current $I_{C,Q}$: The deviation between the measured I_C and the estimated $I_{C,Q}$ increases with the current magnitude [I_C is larger than $I_{C,Q}$, see Fig. 3(a.i)], and hence, the calculated losses according to (4) over estimate the measured power loss in Fig. 3(a.ii). This error could possibly be reduced by directly conducting a Steinmetz fit on the measured losses and the rms MLCC current I_C, which is intended to be done in a follow up study.

Similarly, the impact of dc bias on the model is evaluated in Fig. 3(b) (for an excitation frequency $f = 100$ Hz). Across the full excitation voltage, again, the rms current and loss estimation errors remain below 5% and 25%, respectively.

Therefore, the proposed model—an ESR model based upon the peak-charge based Steinmetz parameters—accurately predicts large-signal MLCC losses from measured current. The improved accuracy of the model is especially stark when compared to a model that utilizes the small-signal ESR value from the datasheet, which can result in an error of up to a factor of ten [12].

IV. Design Example

We apply the proposed—and now validated—model to a practical design example, shown in Fig. 4. Here, MLCCs are used in a full-sinewave filter with a capacitance $C_f = 1.2\ \mu$F for a 3-kW motor drive inverter. This sinewave filter is designed to limit the high-frequency motor stresses of an induction machine (Siemens 1LE1003-1AA42-2NA4-Z H01, $U_{ac} = 230\ V_{rms}$ line-to-neutral voltage, $f = 100$ Hz nominal stator frequency, 5820 r/min nominal speed). The inverter operates with a dc-link voltage U_{in} =800 V and the filter capacitors are referenced to the positive C_{f1} and negative C_{f2} dc-link rail to provide both common- and differential-mode attenuation and to reduce the overall capacitance variation [20], [21].

During operation, both C_{f1} and C_{f2} are subject to a dc bias of $U_{dc} = U_{in}/2$=400 V and peak voltages up to $U_{Cf1,max} = U_{Cf2,max} = U_{in} + \hat{U}_{ac} = 725\ V_{pk}$. At this operating point, the minimum capacitance values of C_{f1} and C_{f2} drop as low as 17% of the nominal capacitance value (see Fig. 1), but the filter structure limits the nonlinearity of the effective capacitance value $C_f = C_{f1} + C_{f2}$ to 32% (with the minimum value occurring at the voltage zero crossing in a motor ac period). Therefore, to achieve a minimum capacitance value $C_f = 1.2\ \mu$F, a total of eight 470 nF MLCCs (i.e., four devices each referenced to the positive and negative dc-link rail) is required.

In the test setup [see Fig. 2(a)] a single MLCC is exposed to the nominal operating point condition for the considered application, i.e., excited with $\hat{U}_C = 325\ V_{pk}/U_{dc} = 400$ V / $f = 100$ Hz), which results in a measured rms current of $I_C = 33\ mA_{rms}$. With this measurement, we can calculate the ESR according to (5) as 171 Ω and calculate per-capacitor losses of 184 mW. Under this same large-signal excitation, the losses are directly measured with the Sawyer–Tower circuit as 176 mW, and the proposed model accurately predicts the losses to within 5% of the measurement. The total filter capacitor losses are 1.5 W per inverter phase and 4.4 W total for the inverter sinewave filter.

Note that the employed Steinmetz parameters were recorded at room temperature (25 °C) while the MLCC losses will cause self-heating above ambient temperature. However, the MLCC losses were found to decrease with increasing temperature by approximately 0.6%/K in [12], so the design approach is conservative and thermal runaway can be ruled out. According to [6], up to 900 mW can be dissipated for the particular MLCC without a temperature increase above 20 °C, so there is sufficient margin for modeling inaccuracies and the MLCC switching/high-frequency losses (see, e.g., [22], [23]), which are typically small compared to the low-frequency large-signal excitation losses in a sinewave filter [12] and hence not considered here.

In some other practical applications, there might be a need to connect capacitors in parallel for handling higher current, and/or in series to handle higher voltages. In case of a parallel connection, the MLCC current excitation is directly defined by the large-signal voltage excitation and the losses can be calculated independently for each device. In the case several devices are connected in series the excitation voltage will be shared—as a first approximation—according to the impedance ratio of the MLCCs, where balancing resistors are required to assure equal dc voltage sharing. Here, the measured rms current flowing through the series connection of the MLCCs can of course be employed to calculate the MLCC losses of each device.

V. Conclusion

MLCCs with ferroelectric Class II dielectrics enable extremely high volumetric capacitance density—and therefore power-dense power converters—but these capacitors suffer from a nonlinear dielectric constant and, in certain applications, substantial large-signal excitation losses. Our previous work introduced a peak-charge-based MLCC Steinmetz-loss model

that accurately described the MLCC power losses under various large-signal operating conditions, including biased and nonsinusoidal excitation voltage waveforms, but this model suffered from the shortcoming that the MLCC peak charge is not easily measured.

In this letter, we proposed and validated a simplified, accurate ESR-based MLCC loss model that calculates the operating-point-specific ESR from *only* Steinmetz parameters and a current measurement, which is much more straightforward than a peak charge measurement. Even under the model assumptions, a loss error between the model and our measurements for a representative ac was below 25% at every considered operating point which is a major improvement compared to a model that utilizes the small-signal ESR value from the datasheet, which can result in an error of up to a factor of ten. In a design example for a sine-wave filter in a 3-kW motor drive inverter, the model was demonstrated to predict losses within 5% of the measured dissipated power.

With an accurate model and a straightforward measurement, these critical losses can be predicted across a range of applications. Steinmetz parameters for a large number of X7R and X7T Class II MLCCs are provided in [13], supporting the fast and broad adoption of the MLCC ESR-based model described in this letter.

REFERENCES

[1] M. Randall, D. Skamser, J. Kinard, and A. Tajuddin, "Thin film MLCC," in *Proc. Symp. Passive Compon.*, 2007, pp. 372–384.

[2] M. J. Pan and C. Randall, "A brief introduction to ceramic capacitors," *IEEE Elect. Insul. Mag.*, vol. 26, no. 3, pp. 44–50, May/Jun. 2010.

[3] K. Syfer, "Syfer application notes," 2014. [Online]. Available: https://www.digikey.ee/en/pdf/k/knowles-syfer/application-notes

[4] Y. Lei et al., "A 2-kW single-phase seven-level flying capacitor multilevel inverter with an active energy buffer," *IEEE Trans. Power Electron.*, vol. 32, no. 11, pp. 8570–8581, Nov. 2017.

[5] D. Bortis, D. Neumayr, and J. W. Kolar, "$\eta\rho$-Pareto optimization and comparative evaluation of inverter concepts considered for the GOOGLE Little Box Challenge," in *Proc. IEEE Workshop Control Model. Power Electron.*, 2016, pp. 1–5.

[6] Johanson Dielectrics, Camarillo, CA, USA, "AC power computations for DC rated capacitors," May 2005. [Online]. Available: https://www.johansondielectrics.com/downloads/ac-power-computations-for-dc-rated-capacitors.pdf

[7] D. Neumayr, D. Bortis, J. W. Kolar, M. Koini, and J. Konrad, "Comprehensive large-signal performance analysis of ceramic capacitors for power pulsation buffers," in *Proc. IEEE Workshop Control Model. Power Electron.*, 2016, pp. 1–8.

[8] C. B. Barth, T. Foulkes, I. Moon, Y. Lei, S. Qin, and R. C. Pilawa-Podgurski, "Experimental evaluation of capacitors for power buffering in single-phase power converters," *IEEE Trans. Power Electron.*, vol. 34, no. 8, pp. 7887–7899, Aug. 2019.

[9] S. Ben-Yaakov, "Some observations on loss and hysteresis of ferroelectric-based ceramic capacitors," *IEEE Trans. Power Electron.*, vol. 33, no. 11, pp. 9127–9129, Nov. 2018.

[10] L. E. Mosley, "Capacitor impedance needs for future microprocessors," in *Proc. Symp. Passive Compon.*, 2006, pp. 168–178.

[11] A. Raciti, S. Rizzo, N. Salerno, G. Susinni, R. Scollo, and A. Scuto, "Modeling the hysteresis power losses of the output parasitic capacitance in super junction MOSFETs," in *Proc. IEEE Int. Symp. Power Electron., Elect. Drives, Automat. Motion*, 2018, pp. 527–532.

[12] D. Menzi, D. Bortis, G. Zulauf, M. Heller, and J. W. Kolar, "Novel iGSE-C loss modelling of X7R ceramic capacitors," *Trans. Power Electron.*, vol. 35, pp. 13367–13383, 2020.

[13] D. Menzi, M. Heller, and J. W. Kolar, "iGSE-C_x A new normalized Steinmetz model for Class II multilayer ceramic capacitors," *IEEE Open J. Power Electron.*, vol. 2, pp. 138–144, 2021.

[14] C. P. Steinmetz, "On the law of hysteresis," *Trans. Amer. Inst. Elect. Engineers*, vol. 9, no. 1, pp. 1–64, 1892.

[15] J. G. Zhu, S. Y. R. Hui, and V. S. Ramsden, "A generalized dynamic circuit model of magnetic cores for low- and high-frequency applications – Part I: Theoretical calculation of the equivalent core loss resistance," *IEEE Trans. Power Electron.*, vol. 11, no. 2, pp. 246–250, Mar. 1996.

[16] J. Yao, Y. Li, H. Zhao, and S. Wang, "Design of CM inductor based on core loss for radiated EMI reduction in power converters," in *Proc. IEEE Appl. Power Electron. Conf. Expo.*, 2019, pp. 2673–2680.

[17] S. Ben-Yaakov, "Modeling ceramic capacitors loss under high DC bias voltage and high current stress," Jun. 2022. [Online]. Available: https://www.youtube.com/watch?v=d00FQxDmWCI

[18] C. B. Sawyer and C. H. Tower, "Rochelle salt as a dielectric," *Phys. Rev.*, vol. 35, pp. 269–273, 1929.

[19] E. A. Pecherskaya, "The use of the Sawyer-Tower method and its modifications to measure the electrical parameters of ferroelectric materials," *Meas. Techn.*, vol. 50, no. 10, pp. 1101–1107, Oct. 2007.

[20] F. Maislinger, H. Ertl, G. Stojcic, and L. Siplika, "Performance of a two-stage actively damped LC filter for GaN/SiC motor inverters," in *Proc. IEEE Int. Conf. Power Electron. Motion Control*, 2018, pp. 177–183.

[21] F. Maislinger, H. Ertl, G. Stojcic, C. Lagler, and F. Holzner, "Design of a 100 kHz wide bandgap inverter for motor applications with active damped sine wave filter," *J. Eng.*, vol. 2019, no. 17, pp. 3766–3771, 2019.

[22] S. Coday and R. C. N. Pilawa-Podgurski, "High accuracy calorimetric measurements and modeling of ceramic capacitor losses under large ripple operation," in *Proc. IEEE Appl. Power Electron. Conf.*, 2020, pp. 188–194.

[23] Y. Jiang, B. Hu, B. Wen, Y. Shen, and T. Long, "Methodology for large-signal loss characterization of ferroelectric Class II MLCC in high-frequency range," in *Proc. IEEE Energy Convers. Congr. Expo.*, 2022, pp. 1–6.